THE JOURNAL OF PHYSICAL CHEMISTRY A
A JOURNAL OF THE AMERICAN CHEMICAL SOCIETY

pubs.acs.org/JPCA Article

Benchmarking of Density Functionals for *Z*-Azoarene Half-Lives via Automated Transition State Search

Daniel M. Adrion, Danil S. Kaliakin,[†] Patrick Neal,[†] and Steven A. Lopez*

Cite This: *J. Phys. Chem. A* 2021, 125, 6474–6485 Read Online

ACCESS | Metrics & More | Article Recommendations | Supporting Information

ABSTRACT: Molecular photoswitches use light to interconvert from a thermodynamically stable isomer into a metastable isomer. Photoswitches have been used in photopharmacology, catalysis, and molecular solar thermal (MOST) materials because of their spatiotemporal activation. Visible-light-absorbing photoswitches are especially attractive because low-energy light minimizes undesired photochemical reactions and enables biological applications. Ideal photoswitches require well-separated absorption spectra for both isomers and long-lived metastable states. However, predicting thermal half-lives with density functional theory is difficult because it requires locating transition structures and chosing an accurate model chemistry. We now report *EZ*-TS; by automatically calculating activation energies for the thermal $Z \rightarrow E$ isomerization. We used 28 density functionals [local spin density approximation, generalized gradient approximation, meta-GGA, hybrid GGA, and hybrid meta-GGA] and five basis sets [6-31G(d), 6-31+G(d,p), 6-311+G(d,p), cc-pVDZ, and aug-cc-pVDZ]. The hybrid GGA functionals performed the best among all tested functionals. We demonstrate that the mean absolute errors of 14 model chemistries approach chemical accuracy.

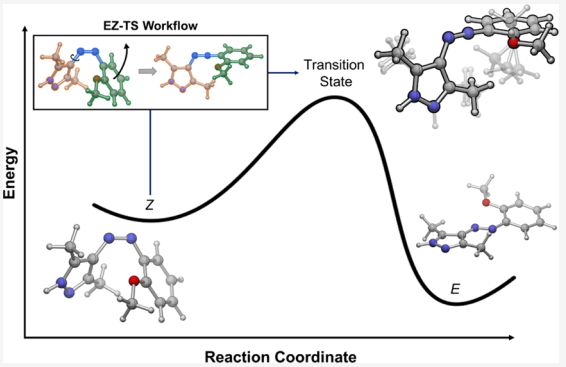

INTRODUCTION

Molecular switches are organic or organometallic molecules that cycle between two distinct chemical states when subjected to outside stimuli, such as changes in pH,[1−6] mechanical force,[7,8] solvent polarity,[9] and light.[10,11] These two states have distinct chemical and physical properties, accessible by switching the stimulus on or off. Light stimulus is easily controlled spatiotemporally and promotes cycling between two photoswitch states. Scheme 1 illustrates the interconversion transition state that depletes the population of the metastable azobenzene *Z* isomer (Scheme 1). Azoarene photoswitches contain two aryl groups flanking the N = N diazo bond; and their switching mechanisms are light-activated. Many classes of photoswitches have emerged in the literature, but azobenzenes are considered prototypical molecular switches because of their relatively straightforward syntheses and reliability but many require ultraviolet light to achieve photoswitching.[12] Replacing the benzene moiety of azobenzene with heteroaryl groups red-shifts the absorbance maxima (λ_{max}) and improves the thermal half-lives over azobenzenes. The relatively low energy of visible light generally avoids undesired photochemical reactions, thus broadening the utility of visible-light photoswitches in biological[13−18] and materials science applications.[19−21] Azoheteroarenes with aryl rings containing nitrogen,[22−26] sulfur,[27−30] and oxygen[31] atoms have been studied. Recent studies by Dreuw and Wegner have shown that thiophenylazobenzene molecules exhibit red-shifted λ_{max} values over azobenzene of up to 60 nm and near-quantitative (>95%) $E \rightarrow Z$ photoswitching when irradiated with visible light.[32] Heindl and Wegner also found in 2020 that substituting the phenyl ring of

Scheme 1. Azobenzene Photoswitching and Thermal Isomerization Reaction (top); Generalized Azoarene Photoswitch, Undergoing $Z \rightarrow E$ Isomerization via an Inversion Mechanism (bottom)

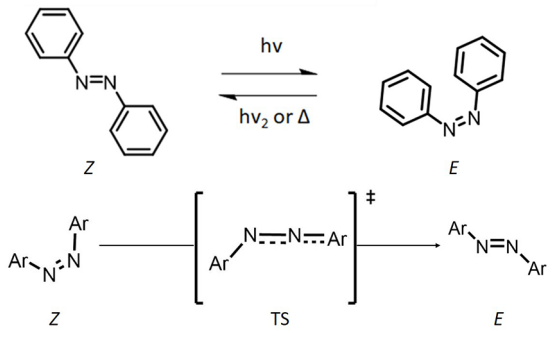

Received: February 24, 2021
Revised: June 18, 2021
Published: July 14, 2021

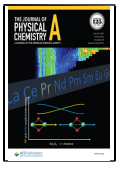

https://doi.org/10.1021/acs.jpca.1c01695
J. Phys. Chem. A 2021, 125, 6474–6485

thiophenylazobenzene with an electron-withdrawing group can stabilize the metastable *Z* isomer and increase the half-life to up to 17.7 h.[33] Azofuran molecules are the least explored of our given examples. A study from 2006 conducted by Oliveira et al. found that a diphenyl furan derivative effectively inhibited the growth of cancer in human cells.[31] The photophysical properties of polymer materials containing a diazofuran moiety were investigated in 2005 by Wang et al.[34] A diazofuran dye molecule was also included in a study conducted in 2000 by Åstrand et al.[35] to investigate the effectiveness of five-membered rings as optical data storage materials. To the best of our knowledge, there have been no studies on the thermal properties of diazofuran molecules to date. Nitrogen-containing photoswitches have by far been the most explored of all heteroaryl photoswitches. These molecules feature improved *Z*-isomer half-lives over azobenzene, ranging from 10 days to 46 years with near-quantitative bidirectional photoswitching (>98% pss).[22,23] The design of next-generation photoswitches is challenging because of the simultaneous tuning of multiple performance parameters: (1) λ_{max}, and the minimal overlap between the absorbance spectrum of the trans- and cis-isomers ($\Delta\lambda_{max}$), (2) the half-life of the relative thermal stability of the metastable isomer ($t_{1/2}$), (3) steady-state relative population of the photostationary states of the stable and metastable isomers, and (4) reproducibility of the switching over time. This paper aims to benchmark 140 model chemistries on their accuracy in predicting azoarene activation free energy barriers ($\Delta G^{\ddagger}$) and introduce a new computational tool to systematically calculate thousands of azoarene transition state structures.

Three possible mechanisms have been put forth to describe the thermal back-isomerization: (1) *rotation* about the CNNC dihedral,[36−38] (2) *inversion*—one side of the π_{NN} bond becomes nearly collinear with one of the aryl rings,[36] and (3) *hula-twist* - the transition structure features a twisting motion about the π_{NN} bond while the aryl groups maintain their relative orientations.[39] Density functional theory (DFT) calculations suggest that the inversion mechanism is generally preferred for the $Z \rightarrow E$ thermal isomerization.[36,40−42] Rietze and co-workers benchmarked density functionals against experimental $\Delta G^{\ddagger}$ for azobenzene and one azobenzene derivative, AzoBiPyB, in 2017.[43] The AzoBiPyB molecule is azobenzene functionalized with pyridines at the meta positions of one benzene. This study benchmarked 13 methods and 7 basis sets, including standard Hartree−Fock calculations, meta-GGA functionals, and range-separated GGA functionals. The authors concluded that both the B3LYP-D3BJ and BMK-D3BJ density functionals with the 6-31G(d) basis set predicted $\Delta G^{\ddagger}$ to be within ∼1 kcal mol^{-1} of experimental values. These studies have shown that the B3LYP functional, coupled with Grimme's dispersion correction D3BJ[44−46] and the 6-31G(d) basis set,[47] provided an acceptable compromise between computational cost and accuracy.[39,40,48]

The limited number of benchmarked model chemistries and molecular scope of azobenzenes has raised doubts on whether B3LYP/6-31G(d) is still the best model chemistry to use. Further, the performance of density functionals cannot be systematically improved; utilizing additional terms or basis functions will not necessarily improve the description of molecular geometries and or energies.[49] Kohn−Sham (KS)-DFT is formally exact, but it involves an exchange−correlation (xc) functional. The xc functional is referred to as a density functional; the exact form of this functional is unknown and essentially unknowable. The KS theory involves parametrizing the electron density by a Slater determinant, which enforces the Pauli exclusion principle and permits the calculation of noninteracting kinetic energy from the orbitals of the Slater determinant as if it were a wave function. The KS orbitals satisfy a set of coupled differential equations similar to the Hartree−Fock (HF) equations of wave function theory (WFT) but containing the xc potential instead of the HF-exchange potential. The xc potential approximates the exchange and includes electron correlation and the electron kinetic energy beyond the noninteracting part(s). All xc functionals have empirical components; these components are often parameters fitted to experimental data and ab initio data and may combine various kinds of empiricism.[50]

Jacob's ladder is an organizational scheme for density functionals with five rungs representing increasing levels of theoretical rigor in xc potentials with higher computational cost.[49,51] From lowest to highest, the rungs are local spin density approximation (LSDA) functionals, generalized gradient approximation (GGA) functionals, meta-GGA functionals, hybrid GGA functionals, and generalized random phase approximation (RPA) functionals.[49] Herein, we include functionals from the first four rungs of Jacob's ladder.

The local spin density approximation (LSDA) functionals are the simplest exchange−correlation functionals, which occupy the first rung of Jacob's ladder. These functionals assume an infinite uniform electron gas. While computationally expedient, these functionals are typically unable to reproduce experimentally measured molecular properties since most molecules and materials have inhomogeneous density distributions. Generalized gradient approximation (GGA) functionals improve upon the systematic errors of the LSDA by introducing a factor that partially accounts for inhomogeneous densities. These functionals occupy the second rung of Jacob's ladder and show significant improvements relative to LSDA. Two additional independent ingredients that further improve the functional's accuracy are the Laplacian of the electron density or the kinetic energy density.[52] The kinetic energy density describes electron delocalization in π-conjugated molecules.[53] The third rung of Jacob's ladder contains functionals with meta-generalized gradient approximations (meta-GGA); meta-GGA functionals include either the Laplacian of the electron density or the kinetic energy.[49] Despite the improvement offered by Laplacian of the electron density or the kinetic energy, self-interaction error (SIE), long-range dynamic correlation (dispersion), and strong correlation cannot be remedied within LSDA, GGA, and meta-GGA.[49] In LSDA, GGA, and meta-GGA the exact exchange term is approximated by the exchange−correlation functional, typically not one-electron SIE-free. Leveraging the description of the exchange term by replacing the local exchange functional with exact HF exchange and using local correlation functional gives zero correlation energy for a one-electron system. Such modification in the treatment of exchange term proved effective in reducing SIE.[54] and has proved effective in improving SIE. Becke pioneered the mixing of a global fraction of exact exchange with the exchange−correlation functional,[46,55] which resulted in a solution that defines Rung 4 of Jacob's ladder (hybrid GGA and hybrid meta-GGA).[49]

COMPUTATIONAL METHODS

We used 28 density functionals featuring hybrid functionals that include Grimme's empirical dispersion corrections (PBE0-

https://doi.org/10.1021/acs.jpca.1c01695
J. Phys. Chem. A 2021, 125, 6474−6485

Scheme 2. *EZ*-TS Workflow Starting from a *cis*-Azoarene SMILES or Coordinate File (Top Left) Generates 12 Transition State Guesses; The Lowest Energy Guess Undergoes a CREST Conformational Search, DFT Conformer Reranking, and Final Conformer Optimizations to Output the Lowest Energy Transition Structure (Bottom Left)

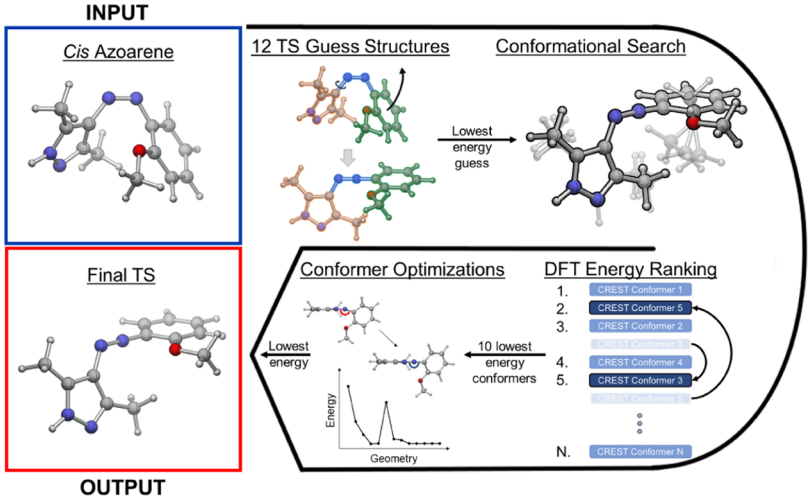

D3BJ,[56] B3LYP-D3BJ,[46,57−59] and BMK-D3BJ[60]), the Petersson−Frisch dispersion correction (APFD),[61] no dispersion corrections (MN12-SX,[62] M06-2X,[63] M06-HF,[64] PBEh1PBE,[65] OHSE2PBE,[66] and mPW1PW91[67]), functionals with long-range corrections (CAM-B3LYP-D3BJ,[68] ωB97X-D,[69] and LC-wHPBE[70]), functionals with generalized gradient approximations (GGA) (M11-L,[71] N12-SX,[62] MPW1B95,[72] mPW1PBE,[67,73] TPSS1KCIS,[74] MPWB1K,[72] MPW1K,[75] BB1K,[76] BHandH,[57,77] ωB97,[78] and ωB97X[78]), the τ-corrected gradient correlation functional TPSSH,[79] and functionals with local spin density approximations (LSDA) (SVWN[80] and SVWN-5[58,80]). We have combined the following five basis sets with each density functional: 6-31G(d), 6-31+G(d,p), 6-311+G(d,p),[47] cc-pVDZ, and aug-cc-pVDZ.[81,82] We included the common double- and triple-Pople family basis sets with and without diffuse functions. We also included correlation-consistent basis sets with and without diffuse functions because they systematically result in smooth convergence of energies toward the complete basis set (CBS) limit with the cardinal number, *n* (in cc-pVnZ). This feature permits the systematic improvement of ab initio energies with basis set size.[83−86] All final optimizations are performed using the Integral Equation Formalism Polarizable Continuum Model[87] (IEFPCM) for Gaussian 16.[88]

DISCUSSION/RESULTS

The purpose of this study is threefold: (1) identify the most accurate model chemistry for predicting the $\Delta G^{\ddagger}$ for the thermal reversion reactions of azoarenes, (2) obtain a clear idea of functional and basis set effects on $\Delta G_{comp}^{\ddagger}$ and thermal isomerization mechanisms, and (3) demonstrate how our open-source *EZ*-TS code can be used to automate thermal isomerization transition structures of diazoarenes. After searching the literature for experimental half-lives and corresponding k_{exp}, we identified many more azoarenes than we could benchmark in a single report. We excluded all azoarenes that featured extended alkyl chains,[89] transition-metal complexes,[90,91] or macrocycles.[92−94] We decided not to include these classes of azoarenes because of the exponentially larger computational cost associated with evaluating the conformational space of alkyl chains and the inconsistent performance of density functionals for organometallic species.[95,96]

***EZ*-TS Open-Access Code.** *EZ*-TS leverages molecular dynamics simulations and DFT calculations to locate the lowest energy transition structure for each $Z \rightarrow E$ isomerization; this workflow is illustrated in Scheme 2.

EZ-TS (available at https://github.com/lopez-lab) first generates the input *cis* azoarene geometry from a simplified molecular-input line-entry system (SMILES)[97] or reads a coordinate file, identifies the central diazo bond, and manipulates the arene fragments to generate 12 transition state guess structures. There are six manipulations performed on either side of the diazo bond wherein each guess is generated by setting one of the CNN angles to 175° and rotating the arene rings relative to each other. These input structures are initially optimized with B3LYP-D3BJ/6-31G(d); a vibrational analysis is performed to verify that the stationary point is indeed a transition structure (one imaginary frequency). We observed that the imaginary frequency for the inversion mechanism is typically in the range of −500 to −250 cm^{-1} for inversion mechanisms. We observed imaginary frequencies in the range of −1500 to −650 cm^{-1} for the rotation mechanism. The lowest-energy guess structure with a frequency between −1500 and −250 cm^{-1} and a CNNC dihedral between 30 and 180° is taken for subsequent calculations. The selected guess structure is subjected to a conformational search with the Conformer Rotamer Ensemble Sampling Tool (CREST),[98] which uses metadynamics simulations to sample the conformational space. Both CNN angles are constrained during the conformer search to maintain the transition state geometry. Additionally, for rotation mechanisms identified by an imaginary frequency less than −650 cm^{-1}, a CNNC dihedral constraint is applied. While the semi empirical GFNn-xTB methods employed by CREST are well parametrized for minima, to ensure that the azoarene transition state conformer ranking was robust, each conformer underwent a rapid 5-step, constrained relaxation in ORCA[99] with B3LYP-D3BJ/6-31G(d) and the RI-JK approximation. After this partial optimization, the conformers are ranked by energy, and the 10 lowest conformers are subjected to an optimization and vibrational analysis procedure using B3LYP-

https://doi.org/10.1021/acs.jpca.1c01695
J. Phys. Chem. A 2021, 125, 6474−6485

Scheme 3. Tested Sets of 11 Azoarene Photoswitches[a]

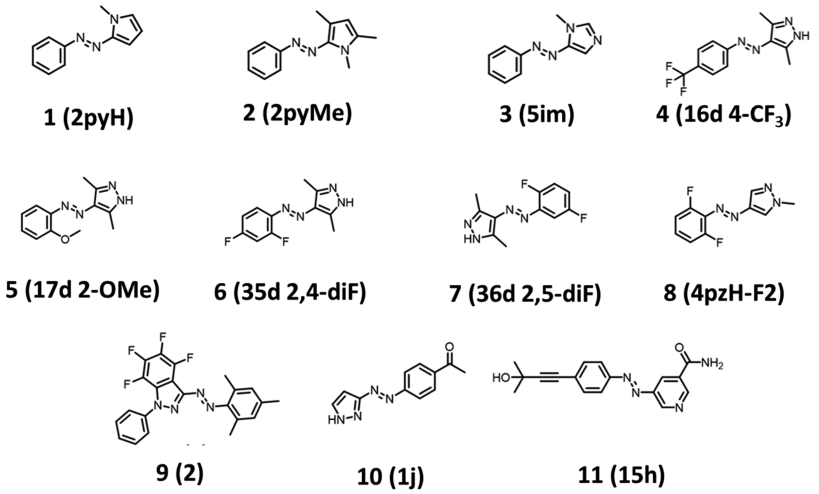

[a]Their labels from the relevant references are given.

D3BJ/6-31G(d) by Gaussian 16. The energies of these 10 conformers are again ranked, discarding nonisomerization transition structures with the same criteria as the guess structures.

With *EZ*-TS in hand, the lowest energy transition state structure at the B3LYP-D3BJ/6-31G(d) level was obtained as the starting point for all benchmarking calculations. This structure was reoptimized with each of the 28 density functionals and 5 basis sets. From each method, an intrinsic reaction coordinate (IRC) calculation was performed on the transition state to yield the corresponding *cis*-azoarene and activation free energy barrier ($\Delta G_{comp}^{\ddagger}$). We report deviations of $\Delta G_{comp}^{\ddagger}$ from $\Delta G_{expt}^{\ddagger}$ as mean absolute error (MAE) for each combination method and basis set. Scheme 3 shows the 11 tested azoarenes and their names in the associated references.

Table 1 shows a summary of the 11 included azoarenes and their corresponding $\Delta G_{expt}^{\ddagger}$, k_{expt}, and known reaction conditions (Solvent and Temperature).

The experimental $\Delta G_{expt}^{\ddagger}$ ranges from 19.5 to 30.1 kcal mol^{-1}, spanning 7 orders of magnitude for rate constants. The large range of rate constants supports our claim of a sufficiently diverse set of azoarenes for a benchmarking study. Next, we begin to assess the performance of all included model chemistries on predicting azoarene $Z \rightarrow E$ thermal isomerization barriers.

Overall Performance. Figure 1 summarizes the MAEs for $\Delta G_{comp}^{\ddagger}$ for each of the 140 model chemistries. The different shapes are organized by basis sets; red corresponds to double-ζ basis sets with diffuse functions (6-31+G(d,p),aug-cc-pVDZ), and black unfilled shapes correspond to 6-31G(d) (black circles) and cc-pVDZ (black triangles). The filled black squares correspond to the 6-311+G(d,p) triple-ζ basis set. The functionals are distributed based on MAE, from largest to smallest.

The MAEs across all functionals ranged from 1.2 to 7.4 kcal mol^{-1}. The best overall performance was achieved by six different model chemistries: B3LYP-D3BJ/6-311+G(d,p), MN12-SX/6-31+G(d,p), MPW1K/6-311+G(d,p), MPW1K/6-31+G(d,p), MPW1B95/6-311+G(d,p), and PBE0-D3BJ/6-311+G(d,p). The worst overall performance was achieved by M06-HF/aug-cc-pVDZ. A visual inspection of the data

Table 1. List of Benchmarked Azoarenes and Corresponding $\Delta G_{expt}^{\ddagger}$ (kcal mol^{-1}), k_{expt} (s^{-1}), and Reaction Conditions (Solvent and Temperature)[a]

azoarene	name in ref	$\Delta G_{expt}^{\ddagger}$	k	conditions
1	**2pyH**[b]	23.1	6.50×10^{-5}	MeCN 25 °C
2	**2pyMe**[b]	19.5	3.30×10^{-2}	MeCN 25 °C
3	**5im**[c]	25.5	1.20×10^{-6}	MeCN 25 °C
4	**16d 4-CF$_3$**[d]	21.9	4.93×10^{-4}	MeCN 25 °C
5	**17d 2-OMe**[d]	23.9	1.73×10^{-5}	MeCN 25 °C
6	**35d 2,4-diF**[d]	23.3	5.43×10^{-5}	MeCN 25 °C
7	**36d 2,5-diF**[d]	20.6	4.72×10^{-3}	MeCN 25 °C
8	**4pzH-F2**[e]	30.1	4.80×10^{-10}	DMSO 25 °C
9	**2**[f]	25.6	1.07×10^{-6}	DMSO 25 °C
10	**1j**[g]	24.2	1.10×10^{-5}	MeOH
11	**15h**[h]	25.1	2.50×10^{-6}	DMSO/H$_2$O (50/50) 25 °C

[a]Standard Transition State Theory (TST) and the Eyring equation were used to convert the rate constants (k) to activation free energy barriers ($\Delta G_{expt}^{\ddagger}$). [b]Weston et al., *J. Am. Chem. Soc.*, **2014**, *136*, 11 878−11 881. [c]Wendler et al., *J. Org. Chem.*, 2012, *77*(7), 3284−3287. [d]Devi et al., *J. Org. Chem.*, **2018**, *83*, 4307−4322. [e]Calbo et al., *Beilstein J. Org. Chem.*, **2019**, *15*, 2753−2764. [f]Traviest-Puente et al., *J. Am. Chem. Soc.*, **2019**, *139*, 3328−3331. [g]Grathwol et al., *ChemMedChem*, **2020**, *15*, 1480−1489. [h]Rustler et al., *J. Org. Chem.*, **2020**, *85*, 4079−4088.

presented in Figure 1 suggests that the choice of density functional affects MAEs more strongly than the basis set. The MAEs have a relatively narrow range across the five basis sets; the PBE0-D3BJ functional yields the smallest range of 0.2 kcal mol^{-1}, while the M06-HF functional affords the largest range (1.7 kcal mol^{-1}). Further, increasing the basis set size from double-ζ (6-31+G(d,p)) to triple-ζ (6-311+G(d,p)) slightly improves average MAE from 2.3 to 2.2 kcal mol^{-1}. We next analyzed the performance of the density functionals with the 6-311+G(d,p) basis set from high to low MAEs. The 10 worst-performing functionals have MAEs that range from 2.1 to 5.7 kcal mol^{-1}. The M06-HF functional gave the highest MAEs, significantly higher than the other functionals. The high MAEs of M06-HF are consistent with respect to the basis set; the

https://doi.org/10.1021/acs.jpca.1c01695
J. Phys. Chem. A 2021, 125, 6474−6485

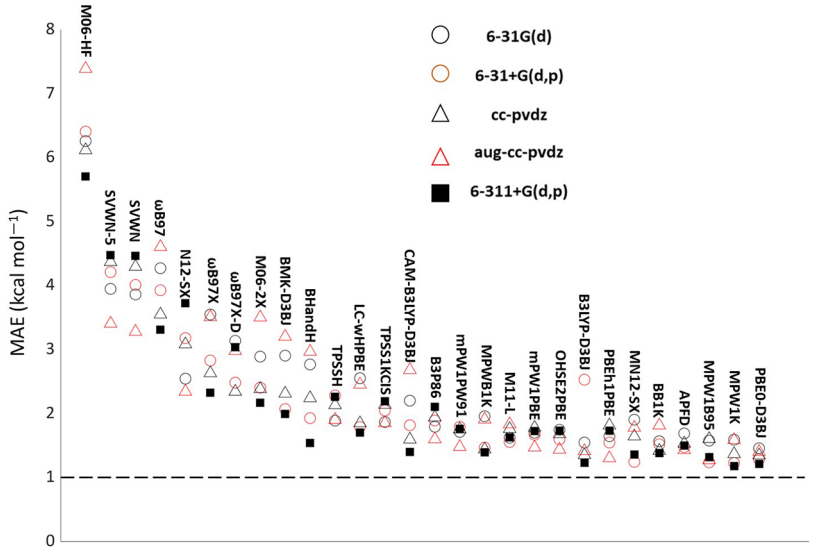

Figure 1. Scatter plot of 140 model chemistries (28 functional and 5 basis set combinations). The 6-31G(d), 6-31+G(d,p), cc-pVDZ, aug-cc-pVDZ, and 6-311+G(d,p) basis set MAEs are shown as the black circles, red circles, black triangles, red triangles, and black squares, respectively. The dotted black line represents the cutoff of chemical accuracy (1.0 kcal mol^{-1}).

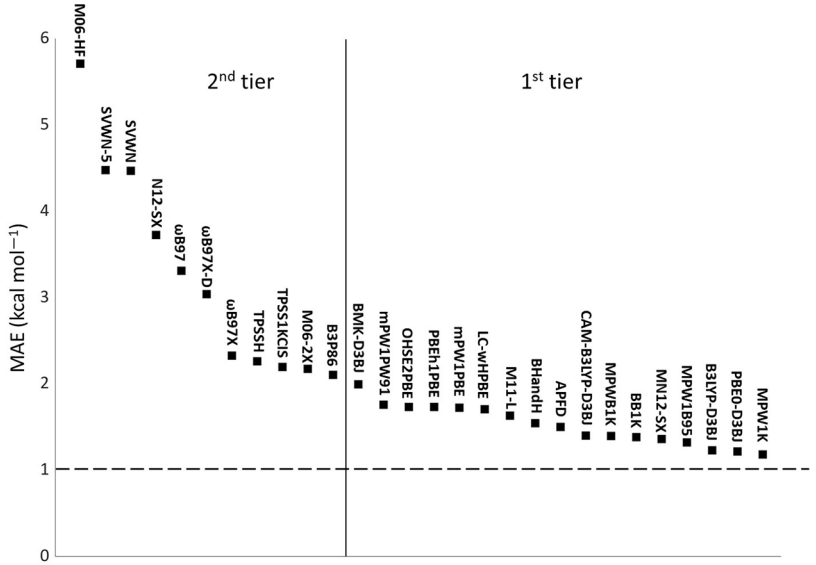

Figure 2. MAE values for each functional with the 6-311+G(d,p) basis set and the two accuracy tiers observed for tested functionals. The MAEs in the first tier are below 2.0 kcal mol^{-1}, and the MAEs in the second tier are above 2.1 kcal mol^{-1}. The dotted black line represents the cutoff of chemical accuracy (1.0 kcal mol^{-1}).

MAEs ranged from a low of 5.9 kcal mol^{-1} (6-311+G(d,p) basis set) to 7.2 kcal mol^{-1} (aug-cc-pVDZ basis set). After M06-HF, the second-worst model chemistry was ωB97/aug-cc-pVDZ with an MAE of 4.6 kcal mol^{-1}.

The best-performing functionals show an MAE range of 1.0−2.0 kcal mol^{-1}. These functionals are PBE0-D3BJ, MN12-SX, CAM-B3LYP-D3BJ, MPW1K, MPWB1K, B3LYP-D3BJ, OHSE2PBE, mPW1PBE, mPW1PW91, PBEh1PBE, M11-L, LC-wHPBE, MPW1B95, BHandH, BMK-D3BJ, BB1K, and APFD. There is also a second tier of functionals, which contains the worse-performing ones (MAEs of 2.1 kcal mol^{-1} and above). The functionals here include SVWN, SVWN-5, M06-2X, M06-HF, N12-SX, B3P86, ωB97, ωB97X, ωB97X-D, TPSSH, and TPSS1KCIS. Next, we will rationalize these tiers of MAEs across all density functionals. Figure 2 shows the MAE of each density functional used with the 6-311+G(d,p) basis set. We use only the triple-ζ basis set for this analysis, as it afforded the lowest MAE when averaged across all functionals.

Both LSDA functionals (SVWN and SVWN-5) are among the highest MAEs (4.5 kcal mol^{-1} for both). The LSDA exchange was developed to approximate HF-exchange. However, because it was derived from the HF-density matrix constructed with the plane wave orbitals of the uniform electron gas, the LSDA exchange functional typically underestimates the exchange energy by 10−15% for inhomogeneous many-electron systems,[46,100] such as azoarenes.

The range-separated functionals (N12-SX, ωB97, ωB97X, and ωB97X-D), with the exception of CAM-B3LYP-D3BJ and LC-wHPBE, were present in the second tier, with ωB97 giving the highest MAE (3.3 kcal mol^{-1}). The standard long-range correction of range-separated functionals features a two-electron operator that is separated into the short-range and

https://doi.org/10.1021/acs.jpca.1c01695
J. Phys. Chem. A 2021, 125, 6474−6485

long-range parts, where conventionally, the short-range part is described with GGA. In contrast, long-range is described with an HF-exchange integral.[101,102] The relatively poor performance of all considered range-separated functionals is a result of long-range-corrected functionals being parametrized in a way that allows for correcting the long-range charge-transfer errors in time-dependent DFT. Such a choice is motivated by the observation that only full HF-exchange properly describes the distance dependence of long-range charge-transfer excitation energies. However, Rohrdanz and Herberta showed that a single range-separation parameter could not provide reasonable accuracy in the prediction of both ground-state properties and vertical excitation energies. The authors explain that acceptable errors in atomization energies and barrier heights are achieved only at the expense of excessively high excitation energies and vice versa.[103]

The two global hybrid GGA functionals that belong to tier 2 and perform poorly relative to the other global hybrids are M06-2X (2.2 kcal mol^{-1}) and M06-HF (5.7 kcal mol^{-1}). The connection between these functionals is the high percentage of HF-exchange compared to the other global hybrids that performed well. To explore the effects of HF-exchange on MAE, we evaluated five hybrid functionals that do not contain dispersion corrections (M06-2X, M06-HF, BHandH, PBEh1PBE, and mPW1PW91). The PBEh1PBE and mPW1PW91 functionals have 25% HF-exchange, while the BHandH, M06-2X, and M06-HF have 50, 54, and 100% of HF-exchange, respectively (Figure 3).

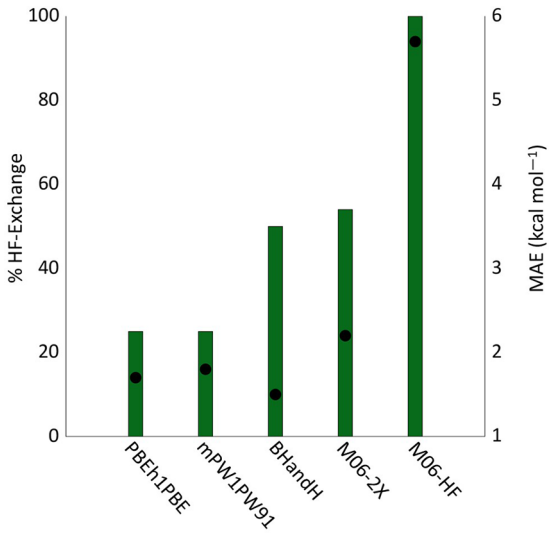

Figure 3. MAE for five hybrid functionals as a function of Hartree−Fock exchange. MAEs are evaluated for the 6-311+G(d,p) basis set. The green bars represent the amount of HF-exchange in each functional, and the black dots represent the MAE in kcal mol^{-1}.

The PBEh1PBE and mPW1PW91 functionals contain 25% HF-exchange and have MAE values of 1.7 and 1.8 kcal mol^{-1}, respectively. From there, the MAEs generally increase along with the amount of HF-exchange. The only exception to this is the BHandH functional, which contains 50% HF-exchange, and has an MAE of 1.5 kcal mol^{-1}. As the amount of HF-exchange increases to 54% in the M06-2X functional, the MAE increased significantly by 0.7 kcal mol^{-1} (2.2 kcal mol^{-1}). Finally, the M06-HF functional (100% HF-exchange) had an MAE of 5.7 kcal mol^{-1}, indicating that the large increase of HF-exchange causes a significant increase in MAEs. This was also the result found in 2017 by Rietze and co-workers, where the exchange-only HF-method gave the largest error in predicting azobenzene thermal reaction kinetics (5.0 kcal mol^{-1}). Moreover, Brothers and co-workers have shown computationally that a large percentage of HF-exchange contributes to increased error for reactions, where there is a rehybridization of bonds in the transition state.[104] Additional analysis was done by systematically altering the amount of HF-exchange for a single functional (PBEh1PBE) and can be found in the Supporting Information.

We now move to an analysis of the first tier (MAEs of 1.9 kcal mol^{-1} and below) of functional performance. The best-performing functionals in this tier approached chemical accuracy (1.0 kcal mol^{-1}) for predicting azoarene thermal isomerization barriers. Some functionals included here are CAM-B3LYP-D3BJ, LC-wHPBE, MN12-SX, and M11-L. As mentioned earlier, the MN12-SX functional performs well (MAE of 1.5 kcal mol^{-1}) because this functional is a range-separated meta-GGA functional that uses the screened exchange (SX) version of range separation, which allows it to overcome the compromise between the accuracy of prediction of excited states energies and ground-state barriers that arise for conventional long-range-corrected range-separated functionals. The LC-wHPBE functional provides accurate MAE (1.5 kcal mol^{-1}). This functional has a lower percentage (20%) of long-range correction compared to other range-separated functionals. Although CAM-B3LYP-D3BJ has a high percentage (33%) of long-range correction, the reasonable performance of this functional in predicting reaction barriers was demonstrated before in a study by Handy and co-workers where they demonstrated that MAE obtained for the BH42/04 dataset[76] is as low as 2.1 kcal mol^{-1}, which is in agreement with MAE of 1.4 kcal mol^{-1} obtained in the present study. The relatively low MAE of 1.6 kcal mol^{-1} calculated with M11-L is most likely due to the high parametrization of this functional compared to the other functionals and the rest of the functionals in the Minnesota family. The M11-L functional has 49 parameters, while B3LYP-D3BJ, ωB97X, M05, M06, and M08-HX functionals have 3, 14, 22, 38, and 44 parameters, respectively.[71]

Other functionals that are in the top tier are PBE0-D3BJ, PBEh1PBE, OHSE2PBE, mPW1PBE, mPW1PW91, MPW1K, and B3LYP-D3BJ. Hybrid meta-GGA functionals of MPW and MPW1 type are among the best-performing functionals, with a range of calculated MAEs between 1.0 and 1.8 kcal mol^{-1}. These results are supported by the work of Zhao and Truhlar in which they demonstrated that MPW1B95 and MPWB1K total mean unsigned errors (TMUEs) for thermochemistry of multiple test sets (AE109/3 atomization energy database,[105] BH42/04 barrier height database,[76] AE6 representative atomization energy database,[106] BH6 representative barrier height database,[106] SPG15/02 saddle point geometries database,[107] ZPE13/99 zero-point energy database,[108] HB4/04 hydrogen bonding database, and WI4/04 weak interaction database) are as low as 1.2 and 1.7 kcal mol^{-1}, respectively.[72] Finally, the class of functionals that performs consistently well in this study are the global hybrid GGA functionals which include PBE0-D3BJ, PBEh1PBE, OHSE2PBE, B3P86, and B3LYP-D3BJ.

The trends established in this study show that the meta-GGA density functionals afford relatively low MAEs (1.4−1.6 kcal mol^{-1}), with M06-2X, TPSSH, and TPSS1KCIS being

https://doi.org/10.1021/acs.jpca.1c01695
J. Phys. Chem. A 2021, 125, 6474−6485

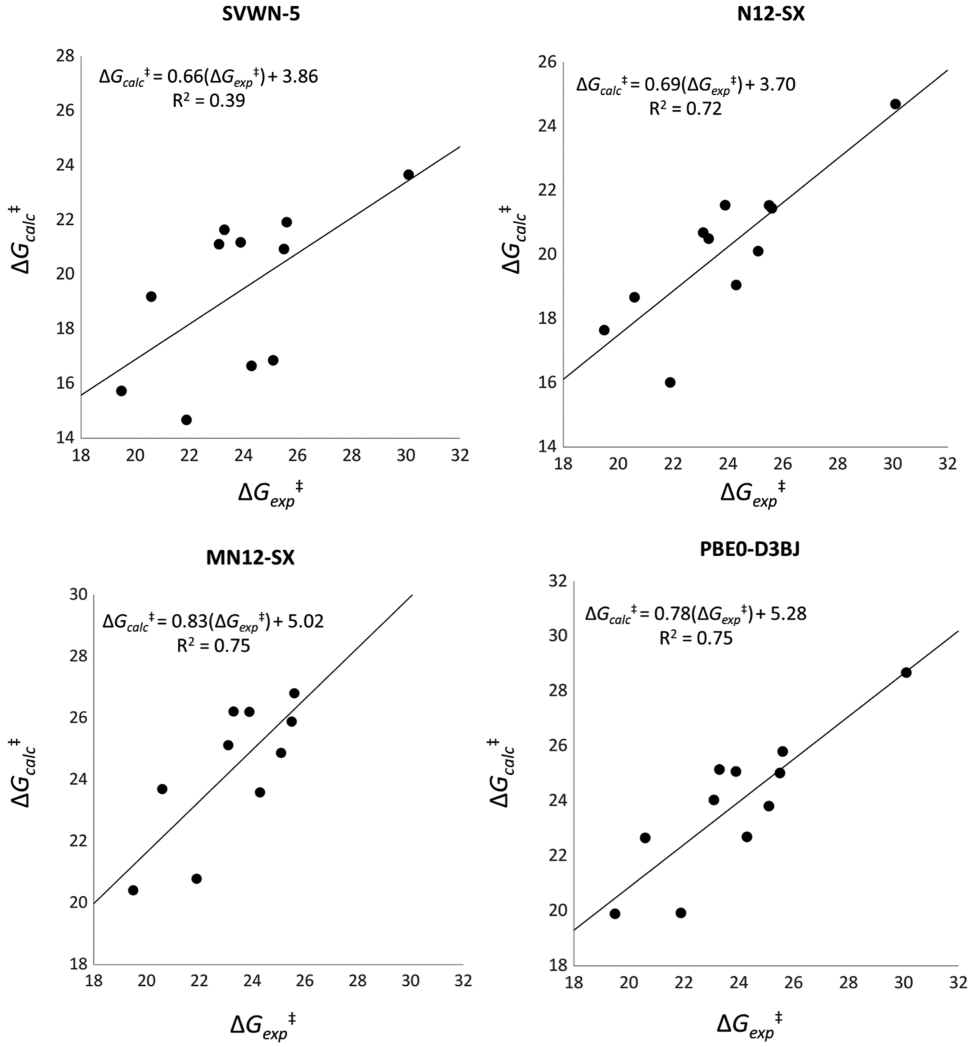

Figure 4. Comparison of experimental and theoretical activation free energies of photoswitches benchmarked in this study. We have included SVWN-5 (LSDA functional, top left), N12-SX (GGA functional, top right), MN12-SX (meta-GGA functional, bottom left), and PBE0-D3BJ (global hybrid functional, bottom right). The lines on each graph represent the line of best fit. The 6-311+G(d,p) basis set was used for all plots.

exceptions (2.2, 2.3, and 2.4 kcal mol^{-1}, respectively). The M06-2X functional contains 54% HF-exchange, whereas the other surveyed meta-GGA functionals contain 42% (BB1K), 25% (MN12-SX), and 0% (M11-L and TPSS1KCIS). LSDA functionals, along with functionals containing a high percentage of HF-exchange, gave high MAEs. We also found that the range-separated functionals afforded relatively large errors, with the CAM-B3LYP-D3BJ and LC-wHPBE functionals being exceptions. GGA functionals also generally gave lower MAEs than meta-GGA functionals. All of these results are for the 6-311+G(d,p) basis set, and the results follow similar trends for the other basis sets (6-31G(d), 6-31+G(d,p), cc-pVDZ, and aug-cc-pVDZ).

Next, we evaluate the performance of our functionals and basis sets in predicting the reactivity of azoarenes used for this study. This analysis aimed to compare the ability of the functionals to measure the relative reactivity of photoswitches. Figure 4 shows the top-performing functionals for each of the first four rungs on Jacob's ladder and their computed and experimentally measured $\Delta G^{\ddagger}$ values. The lines of best fit are presented on each graph, along with their equations and R^2 values.

The SVWN-5 LSDA functional (first rung) had the least consistent azoarene reactivity prediction, with an R^2 of 0.39 and a slope of 0.66. The N12-SX GGA functional (second rung) showed a large performance improvement, with an R^2 of 0.72 and a slope of 0.69. The MN12-SX meta-GGA functional (third rung) had a further improved performance, giving an R^2 of 0.75 and a slope of 0.83. This result coincides with improvement in MAE of the MN12-SX functional over N12-SX (1.4 kcal mol^{-1} to 3.7 kcal mol^{-1}). The PBE0-D3BJ density functional (fourth rung) gave an R^2 of 0.75 (the same as MN12-SX) and a slope of 0.78. Although the PBE0-D3BJ functional gave a slightly lower slope than MN12-SX, it offered an improvement in MAE (1.2 kcal mol^{-1} compared to 1.4 kcal mol^{-1}). We assessed the qualitative performance of the PBE0-D3BJ functional to determine if including diffuse functions to the basis set would improve performance. Figure 5 shows the comparison of experimental and theoretical activation free energies for the PBE0-D3BJ functional with the 6-31G(d), 6-31+G(d,p), cc-pVDZ, and aug-cc-pVDZ basis sets.

Figure 5 shows the basis set effects on the performance of PBE0-D3BJ in predicting azoarene photoswitch reactivity. We first assess the Pople basis sets (top row). The 6-31G(d) basis set performed the worst in predicting reactivity with an R^2 of

https://doi.org/10.1021/acs.jpca.1c01695
J. Phys. Chem. A 2021, 125, 6474−6485

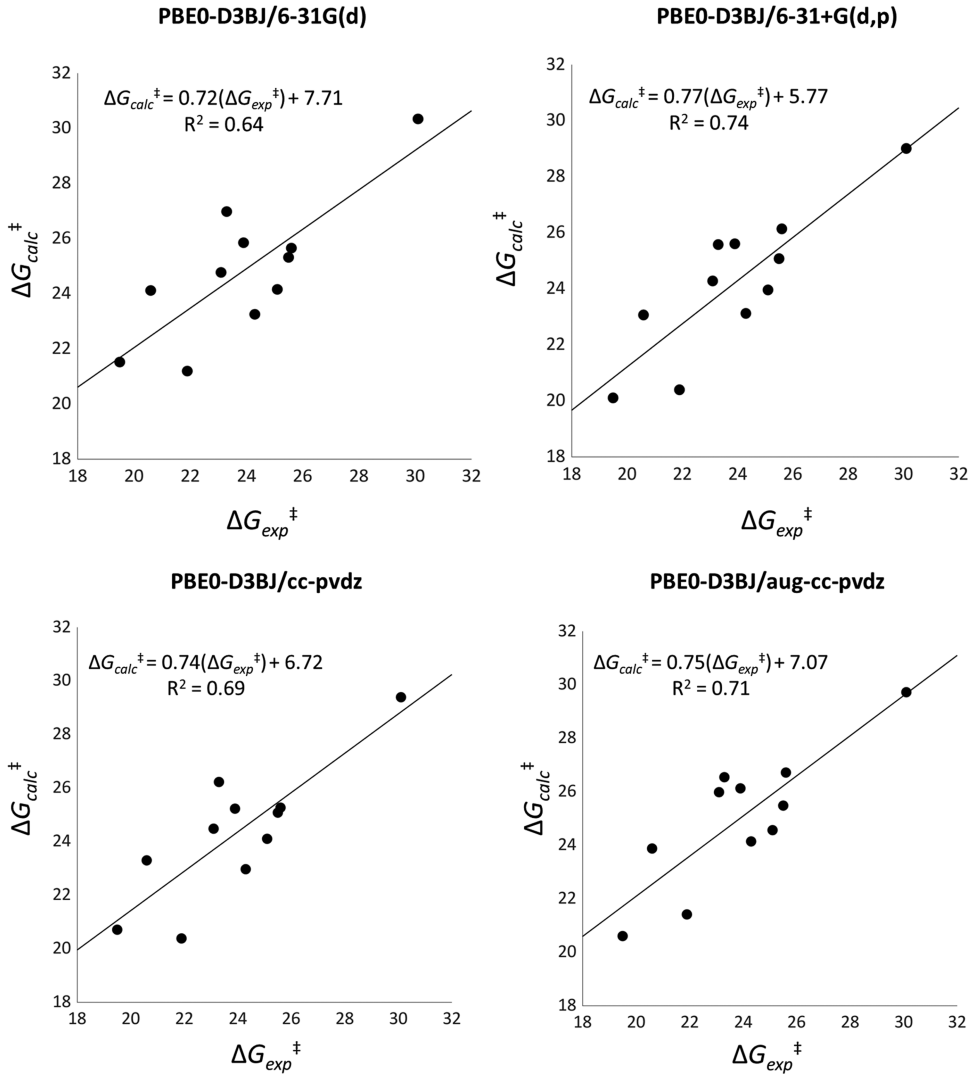

Figure 5. Comparison of experimental and theoretical activation free energies azoarene photoswitches benchmarked in this study. The graphs represent the best-performing functional, PBE0-D3BJ, used with the 6-31G(d) (top left), 6-31+G(d,p) (top right), cc-pVDZ (bottom left), and aug-cc-pVDZ (bottom right) basis sets. The lines on each graph represent the lines of best fit.

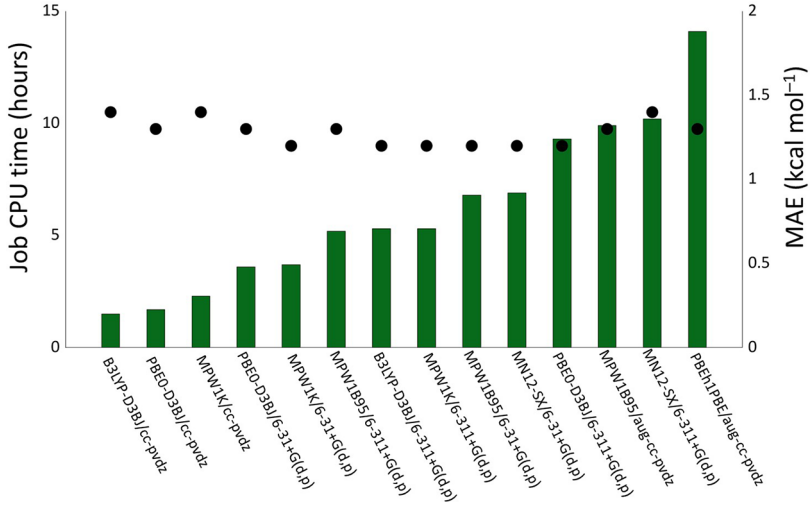

Figure 6. Fourteen top-performing model chemistries for $\Delta G_{comp}^{\ddagger}$. The green bars represent the wall CPU time to complete a vibrational frequency analysis of the transition structures (in hours), and the black dots represent the MAE for a given model chemistry in kcal mol^{-1}.

https://doi.org/10.1021/acs.jpca.1c01695
J. Phys. Chem. A 2021, 125, 6474−6485

0.64. The 6-31+G(d,p) basis set, which adds diffuse functions, offered a significant improvement over 6-31G(d), with an R^2 of 0.74. The 6-311+G(d,p) triple-ζ basis set (Figure 4) performed nearly identical to the 6-31+G(d,p) basis set, giving an R^2 of 0.75. Next, we examine the correlation consistent basis sets cc-pVDZ and aug-cc-pVDZ. The cc-pVDZ basis set had an R^2 value of 0.69. The aug-cc-pVDZ basis set adds diffuse functions to cc-pVDZ and offers a slight improvement, with an R^2 of 0.71. This value is on par with the 6-31+G(d,p) and 6-311+G(d,p) basis sets. All model chemistries including PBE0-D3BJ gave similar slopes when comparing the experimental and theoretical activation free energies (0.72−0.78). The MAE values for the PBE0-D3BJ functional ranged from 1.2 kcal mol^{-1} (6-311+G(d,p) basis set) to 1.5 kcal mol^{-1} (6-31G(d) basis set), suggesting that the absolute deviations from the experimental activation barriers were almost all within an order of magnitude. We then compared the performance of the model chemistries which gave the lowest 10% of MAEs and the CPU times for the frequency calculation of the transition structures (Figure 6).

We focused on this set of 14 model chemistries because they had the lowest MAEs across all 140 computational methods. The range of MAE values in this subset is 0.2 kcal mol^{-1}. Six model chemistries have the minimum MAE value of 1.2 kcal mol^{-1}. They included the B3LYP-D3BJ/6-311+G(d,p), MN12-SX/6-31+G(d,p), MPW1K/6-31+G(d,p), MPW1K /6-31+G(d,p), MPW1B95/6-311+G(d,p), and PBE0-D3BJ/6-311+G(d,p) model chemistries. The highest MAE (1.4 kcal mol^{-1}) of these top-performing methods corresponds to the B3LYP/cc-pVDZ, MPW1K /cc-pVDZ, and MN12-SX/6-311+G(d,p) model chemistries. Four of the five basis sets (6-31+G(d,p), 6-311+G(d,p), cc-pVDZ, and aug-cc-pVDZ) and six of the 28 functionals (PBEh1PBE, MPW1K, PBE0-D3BJ, B3LYP-D3BJ, MPW1B95, and MN12-SX) used in our study are represented in the lowest 10%. The green bars represent the average CPU time for the frequency calculation for each respective model chemistry, ordered from fastest to slowest along the *x*-axis. The black dots represent the average MAE for each model chemistry in kcal mol^{-1}. The shortest average time of 1.5 h was for the B3LYP-D3BJ/cc-pVDZ model chemistry. The longest average time of 14.3 h was for the PBEh1PBE/aug-cc-pVDZ model chemistry. The three shortest average CPU times (1.9−3.6 h) were for model chemistries, including the cc-pVDZ and 6-31+G(d,p) basis sets. The four longest average CPU times (9.3−14.1 h) were all for model chemistries including the 6-311+G(d,p) or aug-cc-pVDZ basis sets. Within these 14 accurate model chemistries, there are no significant increases in accuracy as the computational costs increase. We have shown that any of the six functionals represented here paired with the 6-31+G(d,p) or cc-pVDZ basis sets provide a good balance between cost and accuracy for predicting azoarene thermal activation free energies.

CONCLUSIONS

We provide an automatic computaional framework (*EZ*-TS) to handle 1000 s of quantum mechanical computations to predict activation free energies for azoarene $Z \rightarrow E$ isomerization. We have performed a benchmarking of 28 density functionals and five basis sets for predicting the $\Delta G_{expt}^{\ddagger}$. We included LSDA-type functionals, GGA functionals, meta-GGA functionals, and hybrid functionals with diffuse functions, double-ζ basis sets, and triple-ζ basis sets (Pople and correlation−consistent). We compared our $\Delta G_{comp}^{\ddagger}$ with $\Delta G_{expt}^{\ddagger}$ and calculated the MAE for each model chemistry and molecule. The MAEs ranged from 1.2 kcal mol (achieved by six different model chemistries) to 7.4 kcal mol (M06-HF/aug-cc-pVDZ). The hybrid functionals afforded the lowest MAEs out of all that were tested. The PBE0-D3BJ and MN12-SX functionals with the 6-311+G(d,*p*) basis set best predicted the relative azoarene reactivity (R^2 value of 0.75 and slopes of 0.78−0.83). We identified 14 model chemistries that approach chemical accuracy with MAEs ranging from 1.2 to 1.4 kcal mol^{-1}, with six different model chemistries giving the lowest MAE (1.2 kcal mol^{-1}). The range within the set of lowest 14 model chemistries was small (0.2 kcal mol^{-1}), indicating that any of them would be adequate in predicting $\Delta G_{expt}^{\ddagger}$. With our most accurate model chemistries, we were able to predict azoarene $Z \rightarrow E$ activation barriers within a single order of magnitude and accurately predict the thermal reactivity of the metastable azoarene *Z* isomers. An analysis of the frequency calculation job times for the best-performing model chemistries indicated that using basis sets containing diffuse and triple-ζ basis functions increased the computational time by nearly 10-fold while only offering a relatively small (0.2 kcal mol^{-1}) improvement in MAEs.

ASSOCIATED CONTENT

Supporting Information

The Supporting Information is available free of charge at https://pubs.acs.org/doi/10.1021/acs.jpca.1c01695.

Optimized structures of all optimized transition structures with PBE0-D3BJ/6-311+G(d,p) model chemistry in IEFPCM^{water}; tables of all computed activation free energy barriers for every model chemistry, for all 11 azoarenes; analysis comparing different levels of HF-exchange and its effect on MAE values for the PBEh1PBE functional; analysis comparing the reactant conformational spaces and competing transition state pathways of **2pyH** and **5im** (PDF)

AUTHOR INFORMATION

Corresponding Author

Steven A. Lopez − *Department of Chemistry and Chemical Biology, Northeastern University, Boston, Massachusetts 02115, United States;* orcid.org/0000-0002-8418-3638; Email: s.lopez@northeastern.edu

Authors

Daniel M. Adrion − *Department of Chemistry and Chemical Biology, Northeastern University, Boston, Massachusetts 02115, United States*

Danil S. Kaliakin − *Department of Chemistry and Chemical Biology, Northeastern University, Boston, Massachusetts 02115, United States;* orcid.org/0000-0002-9354-8248

Patrick Neal − *Department of Chemistry and Chemical Biology, Northeastern University, Boston, Massachusetts 02115, United States*

Complete contact information is available at: https://pubs.acs.org/10.1021/acs.jpca.1c01695

Author Contributions

†D.K. and P.N. contributed equally to this work.

Notes

The authors declare no competing financial interest.

https://doi.org/10.1021/acs.jpca.1c01695
J. Phys. Chem. A 2021, 125, 6474−6485

■ ACKNOWLEDGMENTS

S.A.L. acknowledges the Office of Naval Research (ONR N00014-18-1-2659) for funding this research project. D.M.A., D. S. K, and P. N. acknowledge the National Science Foundation (NSF-OAC-1940307) for funding this research. All authors appreciate the assistance from the Northeastern Research Computing Team and access to the computing resources of the Discovery cluster.

■ REFERENCES

(1) Jones, I. M.; Lingard, H.; Hamilton, A. D. pH-Dependent Conformational Switching in 2,6-Benzamidodiphenylacetylenes. *Angew. Chem. Int. Ed.* **2011**, *50*, 12569−12571.
(2) Leblond, J.; Gao, H.; Petitjean, A.; Leroux, J. C. pH-Responsive Molecular Tweezers. *J. Am. Chem. Soc.* **2010**, *132*, 8544−8545.
(3) Muraoka, M.; Irie, H.; Nakatsuji, Y. Acid/base Controllable Molecular Switch Based on a Neutral Phenanthroline Guest Penetrated Pseudorotaxane. *Org. Biomol. Chem.* **2010**, *8*, 2408−2413.
(4) Landge, S. M.; Aprahamian, I. A pH Activated Configurational Rotary Switch: Controlling the E/Z Isomerization in Hydrazones. *J. Am. Chem. Soc.* **2009**, *131*, 18269−18271.
(5) Brazdova, B.; Zhang, N.; Samoshin, V. V.; Guo, X. Trans-2-Aminocyclohexanol as a pH-sensitive Conformational Switch in Lipid Amphiphiles. *Chem. Commun.* **2008**, 4774−4776.
(6) Tuncel, D.; Katterle, M. pH-Triggered Dethreading-Rethreading and Switching of Cucurbit[6]uril on Bistable [3]Pseudorotaxanes and [3]Rotaxanes. *Chem. Eur. J.* **2008**, *14*, 4110−4116.
(7) Walkey, M. C.; Peiris, C. R.; Ciampi, S.; A, C. A.; Dominguez-Espindola, R. B.; Jago, D.; Pulbrook, T.; Skelton, B. W.; Sobolev, A. N.; Diez Perez, I.; Piggott, M. J.; et al. Chemically and Mechanically Controlled Single-Molecule Switches Using Spiropyrans. *ACS Appl. Mater. Interfaces* **2019**, *11*, 36886−36894.
(8) Zhang, Y.; Ma, Y.; Sun, J. Reversible Actuation of Polyelectrolyte Films: Expansion-Induced Mechanical Force Enables Cis-Trans Isomerization of Azobenzenes. *Langmuir* **2013**, *29*, 14919−14925.
(9) Zhou, H.-Y.; Han, Y.; Shi, Q.; Chen, C.-F. A Triply Operable Molecular Switch: Anion-, Acid/Base- and Solvent-Responsive [2]Rotaxane. *Eur. J. Org. Chem.* **2019**, *2019*, 3406−3411.
(10) Bléger, D.; Hecht, S. Visible-Light-Activated Molecular Switches. *Angew. Chem., Int. Ed.* **2015**, *54*, 11338−11349.
(11) Petermayer, C.; Dube, H. Indigoid Photoswitches: Visible Light Responsive Molecular Tools. *Acc. Chem. Res.* **2018**, *51*, 1153−1163.
(12) Crespi, S.; Simeth, N. A.; König, B. Heteroaryl Azo Dyes as Molecular Photoswitches. *Nat. Rev. Chem.* **2019**, *3*, 133−146.
(13) Fehrentz, T.; Schonberger, M.; Trauner, D. Optochemical Genetics. *Angew. Chem. Int. Ed.* **2011**, *50*, 12156−12182.
(14) Broichhagen, J.; Podewin, T.; Meyer-Berg, H.; von Ohlen, Y.; Johnston, N. R.; Jones, B. J.; Bloom, S. R.; Rutter, G. A.; Hoffmann-Roder, A.; Hodson, D. J.; et al. Optical Control of Insulin Secretion Using an Incretin Switch. *Angew. Chem. Int. Ed.* **2015**, *54*, 15565−15569.
(15) Laprell, L.; Repak, E.; Franckevicius, V.; Hartrampf, F.; Terhag, J.; Hollmann, M.; Sumser, M.; Rebola, N.; DiGregorio, D. A.; Trauner, D. Optical Control of NMDA Receptors with a Diffusible Photoswitch. *Nat. Commun.* **2015**, *6*, No. 8076.
(16) Hüll, K.; Morstein, J.; Trauner, D. In Vivo Photopharmacology. *Chem. Rev.* **2018**, *118*, 10710−10747.
(17) Tochitsky, I.; Kienzler, M. A.; Isacoff, E.; Kramer, R. H. Restoring Vision to the Blind with Chemical Photoswitches. *Chem. Rev.* **2018**, *118*, 10748−10773.
(18) Albert, L.; Vazquez, O. Photoswitchable Peptides for Spatiotemporal Control of Biological Functions. *Chem. Commun.* **2019**, *55*, 10192−10213.
(19) Hernandez, J. V.; Kay, E. R.; Leigh, D. A. A Reversible Synthetic Rotary Molecular Motor. *Science* **2004**, *306*, 1532−1537.
(20) Dattler, D.; Fuks, G.; Heiser, J.; Moulin, E.; Perrot, A.; Yao, X.; Giuseppone, N. Design of Collective Motions from Synthetic Molecular Switches, Rotors, and Motors. *Chem. Rev.* **2020**, *120*, 310−433.
(21) Gerwien, A.; Mayer, P.; Dube, H. Green Light Powered Molecular State Motor Enabling Eight-shaped Unidirectional Rotation. *Nat. Commun.* **2019**, *10*, No. 4449.
(22) Calbo, J.; Weston, C. E.; White, A. J.; Rzepa, H. S.; Contreras-Garcia, J.; Fuchter, M. J. Tuning Azoheteroarene Photoswitch Performance through Heteroaryl Design. *J. Am. Chem. Soc.* **2017**, *139*, 1261−1274.
(23) Calbo, J.; Thawani, A. R.; Gibson, R. S. L.; White, A. J. P.; Fuchter, M. J. A Combinatorial Approach to Improving the Performance of Azoarene Photoswitches. *Beilstein J. Org. Chem.* **2019**, *15*, 2753−2764.
(24) Kortekaas, L.; Simke, J.; Kurka, D. W.; Ravoo, B. J. Rapid Photoswitching of Low Molecular Weight Arylazoisoxazole Adhesives. *ACS Appl. Mater. Interfaces* **2020**, *12*, 32054−32060.
(25) Kumar, P.; Srivastava, A.; Sah, C.; Devi, S.; Venkataramani, S. Arylazo-3,5-dimethylisoxazoles: Azoheteroarene Photoswitches Exhibiting High Z-Isomer Stability, Solid-State Photochromism, and Reversible Light-Induced Phase Transition. *Chem. Eur. J.* **2019**, *25*, 11924−11932.
(26) Čechová, L.; Filo, J.; Dracinsky, M.; Slavov, C.; Sun, D.; Janeba, Z.; Slanina, T.; Wachtveitl, J.; Prochazkova, E.; Cigan, M. Polysubstituted 5-Phenylazopyrimidines: Extremely Fast Non-ionic Photochromic Oscillators. *Angew. Chem. Int. Ed.* **2020**, *59*, 15590−15594.
(27) Coelho, P. J.; Castro, M. C. R.; Fernandes, S. S. M.; Fonseca, A. M. C.; Raposo, M. M. M. Enhancement of the Photochromic Switching Speed of Bithiophene Azo Dyes. *Tetrahedron Lett.* **2012**, *53*, 4502−4506.
(28) Coelho, P. J.; Carvalho, L. M.; Moura, J. C. V. P.; Raposo, M. M. M. Novel Photochromic 2,2′-Bithiophene Azo Dyes. *Dyes Pigm.* **2009**, *82*, 130−133.
(29) Jaunet-Lahary, T.; Chantzis, A.; Chen, K. J.; Laurent, A. D.; Jacquemin, D. Designing Efficient Azobenzene and Azothiophene Nonlinear Optical Photochromes. *J. Phys. Chem. C* **2014**, *118*, 28831−28841.
(30) Huddleston, P. R.; Volkov, V. V.; Perry, C. C. The Structural and Electronic Properties of 3,3'-Azothiophene Photo-Switching Systems. *Phys. Chem. Chem. Phys.* **2019**, *21*, 1344−1353.
(31) de Oliveira, R. B.; de Souza-Fagundes, E. M.; Siqueira, H. A.; Leite, R. S.; Donnici, C. L.; Zani, C. L. Synthesis and Evaluation of Cytotoxic Activity of Arylfurans. *Eur. J. Med. Chem.* **2006**, *41*, 756−760.
(32) Slavov, C.; Yang, C.; Heindl, A. H.; Wegner, H. A.; Dreuw, A.; Wachtveitl, J. Thiophenylazobenzene: An Alternative Photoisomerization Controlled by Lone-Pairpi. *Angew. Chem. Int. Ed.* **2020**, *59*, 380−387.
(33) Heindl, A. H.; Wegner, H. A. Rational Design of Azothiophenes-Substitution Effects on the Switching Properties. *Chem. Eur. J.* **2020**, *26*, 13730−13737.
(34) Wang, Y.; Ma, J.; Jiang, Y. Tuning of Electronic Structures of Poly(p-phenylenevinylene) Analogues of Phenyl, Thienyl, Furyl, and Pyrrolyl by Double-bond Linkages of Group 14 and 15 Elements. *J. Phys. Chem. A* **2005**, *109*, 7197−7206.
(35) Åstrand, P.-O.; Sommer-Larsen, P.; Hvilsted, S.; Ramanujam, P. S.; Bak, K. L.; Sauer, S. P. A. Five-membered Rings as Diazo Components in Optical Data Storage Devices: an ab initio Investigation of the Lowest Singlet Excitation Energies. *Chem. Phys. Lett.* **2000**, *325*, 115−119.
(36) Crecca, C. R.; Roitberg, A. E. Theoretical Study of the Isomerization Mechanism of Azobenzene and Disubstituted Azobenzene Derivatives. *J. Phys. Chem. A* **2006**, *110*, 8188−203.
(37) He, Y.; Shangguan, Z.; Zhang, Z. Y.; Xie, M.; Yu, C.; Li, T. Azobispyrazole Family as Photoswitches Combining (Near-)-Quantitative Bidirectional Isomerization and Widely Tunable Thermal Half-Lives from Hours to Years. *Angew. Chem., Int. Ed.* **2021**, *60*, 2−10.

https://doi.org/10.1021/acs.jpca.1c01695
J. Phys. Chem. A 2021, 125, 6474−6485

(38) Gagliardi, L.; Orlandi, G.; Bernardi, F.; Cembran, A.; Garavelli, M. A Theoretical Study of the Lowest Electronic States of Azobenzene: The Role of Torsion Coordinate in the cis−trans Photoisomerization. *Theor. Chem. Acc.* **2004**, *111*, 363−372.
(39) Muždalo, A.; Saalfrank, P.; Vreede, J.; Santer, M. Cis-to-Trans Isomerization of Azobenzene Derivatives Studied with Transition Path Sampling and Quantum Mechanical/Molecular Mechanical Molecular Dynamics. *J. Chem. Theory Comput.* **2018**, *14*, 2042−2051.
(40) Dokić, J.; Gothe, M.; Wirth, J.; Peters, M. V.; Schwarz, J.; Hecht, S.; Saalfrank, P. Quantum Chemical Investigation of Thermal cis-to-trans Isomerization of Azobenzene Derivatives: Substituent Effects, Solvent Effects, and Comparison to Experimental Data. *J. Phys. Chem. A* **2009**, *113*, 6763−6773.
(41) Robertus, J.; Reker, S. F.; Pijper, T. C.; Deuzeman, A.; Browne, W. R.; Feringa, B. L. Kinetic Analysis of the Thermal Isomerisation Pathways in an Asymmetric Double Azobenzene Switch. *Phys. Chem. Chem. Phys.* **2012**, *14*, 4374−4382.
(42) Asano, T.; Okada, T.; Shinkai, S.; Shigematsu, K.; Kusano, Y.; Manabe, O. Temperature and Pressure Dependences of Thermal cis-to-trans Isomerization of Azobenzenes which Evidence an Inversion Mechanism. *J. Am. Chem. Soc.* **1981**, *103*, 5161−5165.
(43) Rietze, C.; Titov, E.; Lindner, S.; Saalfrank, P. Thermal Isomerization of Azobenzenes: On the Performance of Eyring Transition State Theory. *J. Phys. Condens. Matter.* **2017**, *29*, No. 314002.
(44) Hertwig, R. H.; Koch, W. On the Parameterization of the Local Correlation Functional. What is Becke-3-LYP? *Chem. Phys. Lett.* **1997**, *268*, 345−351.
(45) Grimme, S.; Ehrlich, S.; Goerigk, L. Effect of the Damping Function in Dispersion Corrected Density Functional Theory. *J. Comput. Chem.* **2011**, *32*, 1456−1465.
(46) Becke, A. D. Density-functional thermochemistry. III. The role of Exact Exchange. *J. Chem. Phys.* **1993**, *98*, 5648−5652.
(47) Ditchfield, R.; Hehre, W. J.; Pople, J. A. Self-Consistent Molecular-Orbital Methods. IX. An Extended Gaussian-Type Basis for Molecular-Orbital Studies of Organic Molecules. *J. Chem. Phys.* **1971**, *54*, 724−728.
(48) Biswas, N.; Umapathy, S. Density Functional Calculations of Structures, Vibrational Frequencies, and Normal Modes oftrans-andcis-Azobenzene. *J. Phys. Chem. A* **1997**, *101*, 5555−5566.
(49) Mardirossian, N.; Head-Gordon, M. Thirty Years of Density Functional Theory in Computational Chemistry: An Overview and Extensive Assessment of 200 Density Functionals. *Mol. Phys.* **2017**, *115*, 2315−2372.
(50) Peverati, R.; Truhlar, D. G. Quest for a Universal Density Functional: The Accuracy of Density Functionals Across a Broad Spectrum of Databases in Chemistry and Physics. *Philos. Trans. A Math. Phys. Eng. Sci.* **2014**, *372*, No. 20120476.
(51) Perdew, J. P.; Ruzsinszky, A.; Tao, J.; Staroverov, V. N.; Scuseria, G. E.; Csonka, G. I. Prescription for the Design and Selection of Density Functional Approximations: More Constraint Satisfaction with Fewer Fits. *J. Chem. Phys.* **2005**, *123*, No. 062201.
(52) Perdew, J. P.; Constantin, L. A. Laplacian-level Density Functionals for the Kinetic Energy Density and Exchange-correlation Energy. *Phys. Rev. B* **2007**, *75*, DOI: 10.1103/PhysRevB.75.155109.
(53) Schmider, H. L.; Becke, A. D. Chemical Content of the Kinetic Energy Density. *J. Mol. Struct.: THEOCHEM* **2000**, *527*, 51−61.
(54) Perdew, J. P.; McMullen, E. R.; Zunger, A. Density-Functional Theory of the Correlation Energy in Atoms and Ions: A Simple Analytic Model and a Challenge. *Phys. Rev. A* **1981**, *23*, 2785−2789.
(55) Becke, A. D. A new mixing of Hartree−Fock and Local Density-Functional Theories. *J. Chem. Phys.* **1993**, *98*, 1372−1377.
(56) Adamo, C.; Barone, V. Toward Reliable Density Functional Methods without Adjustable Parameters: The PBE0 Model. *J. Chem. Phys.* **1999**, *110*, 6158−6170.
(57) Lee, C.; Yang, W.; Parr, R. G. Development of the Colle-Salvetti Correlation-Energy Formula into a Functional of the Electron Density. *Phys. Rev. B* **1988**, *37*, 785−789.
(58) Vosko, S. H.; Wilk, L.; Nusair, M. Accurate Spin-Dependent Electron Liquid Correlation Energies for Local Spin Density Calculations: A Critical Analysis. *Can. J. Phys.* **1980**, *58*, 1200−1211.
(59) Stephens, P. J.; Devlin, F. J.; Chabalowski, C. F.; Frisch, M. J. Ab Initio Calculation of Vibrational Absorption and Circular Dichroism Spectra Using Density Functional Force Fields. *J. Phys. Chem. A* **1994**, *98*, 11623−11627.
(60) Boese, A. D.; Martin, J. M. Development of Density Functionals for Thermochemical Kinetics. *J. Chem. Phys.* **2004**, *121*, 3405−3416.
(61) Austin, A.; Petersson, G. A.; Frisch, M. J.; Dobek, F. J.; Scalmani, G.; Throssell, K. A Density Functional with Spherical Atom Dispersion Terms. *J. Chem. Theory Comput.* **2012**, *8*, 4989−5007.
(62) Peverati, R.; Truhlar, D. G. Screened-Exchange Density Functionals with Broad Accuracy for Chemistry and Solid-State Physics. *Phys. Chem. Chem. Phys.* **2012**, *14*, 16187−16191.
(63) Zhao, Y.; Truhlar, D. G. The M06 Suite of Density functionals for Main Group Thermochemistry, Thermochemical Kinetics, Noncovalent Interactions, Excited States, and Transition Elements: Two New Functionals and Systematic Testing of Four M06-Class Functionals and 12 Other Functionals. *Theor. Chem. Acc.* **2007**, *120*, 215−241.
(64) Zhao, Y.; Truhlar, D. G. Density Functional for Spectroscopy: No Long-Range Self-Interaction Error, Good Performance for Rydberg and Charge-Transfer States, and better Performance on Average than B3LYP for Ground States. *J. Phys. Chem. A* **2006**, *110*, 13126−30.
(65) Ernzerhof, M.; Perdew, J. P. Generalized Gradient Approximation to the Angle- and System-Averaged Exchange Hole. *J. Chem. Phys.* **1998**, *109*, 3313−3320.
(66) Heyd, J.; Scuseria, G. E.; Ernzerhof, M. Hybrid Functionals Based on a Screened Coulomb Potential. *J. Chem. Phys.* **2003**, *118*, 8207−8215.
(67) Adamo, C.; Barone, V. ExchangeFfunctionals with Improved Long-Range Behavior and Adiabatic Connection Methods without Adjustable Parameters: The mPW and mPW1PW Models. *J. Chem. Phys.* **1998**, *108*, 664−675.
(68) Yanai, T.; Tew, D. P.; Handy, N. C. A New Hybrid Exchange−Correlation Functional Using the Coulomb-Attenuating Method (CAM-B3LYP). *Chem. Phys. Lett.* **2004**, *393*, 51−57.
(69) Chai, J. D.; Head-Gordon, M. Long-Range Corrected Hybrid Density Functionals with Damped Atom-Atom Dispersion Corrections. *Phys. Chem. Chem. Phys.* **2008**, *10*, 6615−6620.
(70) Henderson, T. M.; Izmaylov, A. F.; Scalmani, G.; Scuseria, G. E. Can Short-Range Hybrids Describe Long-Range-Dependent Properties? *J. Chem. Phys.* **2009**, *131*, No. 044108.
(71) Peverati, R.; Truhlar, D. G. M11-L: A Local Density Functional That Provides Improved Accuracy for Electronic Structure Calculations in Chemistry and Physics. *J. Phys. Chem. Lett.* **2012**, *3*, 117−124.
(72) Zhao, Y.; Truhlar, D. G. Hybrid Meta Density Functional Theory Methods for Thermochemistry, Thermochemical Kinetics, and Noncovalent Interactions: The MPW1B95 and MPWB1K Models and Comparative Assessments for Hydrogen Bonding and van der Waals Interactions. *J. Phys. Chem. A* **2004**, *108*, 6908−6918.
(73) Perdew, J. P.; Burke, K.; Ernzerhof, M. Generalized Gradient Approximation Made Simple. *Phys. Rev. Lett.* **1996**, *77*, 3865−3868.
(74) Zhao, Y.; Lynch, B. J.; Truhlar, D. G. Multi-Coefficient Extrapolated Density Functional Theory for Thermochemistry and Thermochemical Kinetics. *Phys. Chem. Chem. Phys.* **2005**, *7*, No. 43.
(75) Lynch, B. J.; Fast, P. L.; Harris, M.; Truhlar, D. G. Adiabatic Connection for Kinetics. *J. Phys. Chem. A* **2000**, *104*, 4811−4815.
(76) Peach, M. J. G.; Helgaker, T.; Sałek, P.; Keal, T. W.; Lutnæs, O. B.; Tozer, D. J.; Handy, N. C. Assessment of a Coulomb-Attenuated Exchange-Correlation Energy Functional. *Phys. Chem. Chem. Phys.* **2006**, *8*, 558−562.
(77) Becke, A. D. Density-Functional Exchange-Energy Approximation with Correct Asymptotic Behavior. *Phys. Rev. A* **1988**, *38*, 3098−3100.

(78) Chai, J. D.; Head-Gordon, M. Systematic Optimization of Long-Range Corrected Hybrid Density Functionals. *J. Chem. Phys.* **2008**, *128*, No. 084106.
(79) Tao, J.; Perdew, J. P.; Staroverov, V. N.; Scuseria, G. E. Climbing the Density Functional Ladder: Nonempirical Meta-Generalized Gradient Approximation Designed for Molecules and Solids. *Phys. Rev. Lett.* **2003**, *91*, No. 146401.
(80) Slater, J. C.; Phillips, J. C. Quantum Theory of Molecules and Solids Vol. 4: The Self-Consistent Field for Molecules and Solids. *Phys. Today* **1974**, *27*, 49−50.
(81) Woon, D. E.; Dunning, T. H. Gaussian Basis Sets for Use in Correlated Nolecular Calculations. V. Core-valence basis sets for boron through neon. *J. Chem. Phys.* **1995**, *103*, 4572−4585.
(82) Kendall, R. A.; Dunning, T. H.; Harrison, R. J. Electron Affinities of the First-Row Atoms Revisited. Systematic Basis Sets and Wave Functions. *J. Chem. Phys.* **1992**, *96*, 6796−6806.
(83) Feller, D.; Dixon, D. A. Density Functional Theory and the Basis Set Truncation Problem with Correlation Consistent Basis Sets: Elephant in the Room or Mouse in the Closet? *J. Phys. Chem. A* **2018**, *122*, 2598−2603.
(84) Ranasinghe, D. S.; Petersson, G. A. CCSD(T)/CBS Atomic and Molecular Benchmarks for H Through Ar. *J. Chem. Phys.* **2013**, *138*, No. 144104.
(85) Martin, J. M. L. On the Performance of Correlation Consistent Basis Sets for the Calculation of Total Atomization Energies, Geometries, and Harmonic Frequencies. *J. Chem. Phys.* **1994**, *100*, 8186−8193.
(86) Sylvetsky, N.; Kesharwani, M. K.; Martin, J. M. L. The aug-cc-pVnZ-F12 Basis Set Family: Correlation Consistent Basis Sets for Explicitly Correlated Benchmark Calculations on Anions and Noncovalent Complexes. *J. Chem. Phys.* **2017**, *147*, No. 134106.
(87) Tomasi, J.; Mennucci, B.; Cammi, R. Quantum Mechanical Continuum Solvation Models. *Chem. Rev.* **2005**, *105*, 2999−3093.
(88) Frisch, M. J.; Trucks, G. W.; Schlegel, H. B.; Scuseria, G. E.; Robb, M. A.; Cheeseman, J. R.; Scalmani, G.; Barone, V.; Petersson, G. A.; Nakatsuji, H.. et al.*Gaussian 16 Rev. C.01*.Wallingford, CT, 2016.
(89) Heindl, A. H.; Wende, R. C.; Wegner, H. A. London Dispersion as Important Factor for the Stabilization of (*Z*)-Azobenzenes in the Presence of Hydrogen Bonding. *Beilstein J. Org. Chem.* **2018**, *14*, 1238−1243.
(90) Li, G.; Ma, X.; Jia, C.; Han, Q.; Wang, Y.; Wang, J.; Yu, L.; Yang, S. Ruthenium-Catalyzed Meta/Ortho-Selective C-H Alkylation of Azoarenes Using Alkyl Bromides. *Chem Commun.* **2017**, *53*, 1261−1264.
(91) Powers, I. G.; Andjaba, J. M.; Luo, X.; Mei, J.; Uyeda, C. Catalytic Azoarene Synthesis from Aryl Azides Enabled by a Dinuclear Ni Complex. *J. Am. Chem. Soc.* **2018**, *140*, 4110−4118.
(92) Vela, S.; Scheidegger, A.; Fabregat, R.; Corminboeuf, C. Tuning the Thermal Stability and Photoisomerization of Azoheteroarenes through Macrocycle Strain*. *Chem. - Eur. J.* **2021**, *27*, 419−426.
(93) Slavov, C.; Yang, C.; Heindl, A. H.; Stauch, T.; Wegner, H. A.; Dreuw, A.; Wachtveitl, J. Twist and Return-Induced Ring Strain Triggers Quick Relaxation of a (*Z*)-Stabilized Cyclobisazobenzene. *J. Phys. Chem. Lett.* **2018**, *9*, 4776−4781.
(94) Bassotti, E.; Carbone, P.; Credi, A.; Di Stefano, M.; Masiero, S.; Negri, F.; Orlandi, G.; Spada, G. P. Effect of Strain on the Photoisomerization and Stability of a Congested Azobenzenophane: A Combined Experimental and Computational Study. *J. Phys. Chem. A* **2006**, *110*, 12385−12394.
(95) Cramer, C. J.; Truhlar, D. G. Density Functional Theory for Transition Metals and Transition Metal Chemistry. *Phys. Chem. Chem. Phys.* **2009**, *11*, 10757−10816.
(96) Qi, S.-C.; Hayashi, J.-i.; Zhang, L. Recent Application of Calculations of Metal Complexes Based on Density Functional Theory. *RSC Adv.* **2016**, *6*, 77375−77395.
(97) Weininger, D. SMILES, a Chemical Language and Information System. 1. Introduction to Methodology and Encoding Rules. *J. Chem. Inf. Model.* **1988**, *28*, 31−36.
(98) Pracht, P.; Bohle, F.; Grimme, S. Automated Exploration of the Low-Energy Chemical Space with Fast Quantum Chemical Methods. *Phys. Chem. Chem. Phys.* **2020**, *22*, 7169−7192.
(99) Neese, F. The ORCA program system. *WIREs Comput. Mol. Sci.* **2012**, *2*, 73−78.
(100) Kang, J. K.; Musgrave, C. B. Prediction of Transition State Barriers and Enthalpies of Reaction by a New Hybrid Density-Functional Approximation. *J. Chem. Phys.* **2001**, *115*, 11040−11051.
(101) Iikura, H.; Tsuneda, T.; Yanai, T.; Hirao, K. A Long-Range Correction Scheme for Generalized-Gradient-Approximation Exchange Functionals. *J. Chem. Phys.* **2001**, *115*, 3540−3544.
(102) Adamson, R. D.; Dombroski, J. P.; Gill, P. M. W. Efficient Calculation of Short-Range Coulomb Energies. *J. Comput. Chem.* **1999**, *20*, 921−927.
(103) Rohrdanz, M. A.; Herbert, J. M. Simultaneous Benchmarking of Ground- and Excited-State Properties with Long-Range-Corrected Density Functional Theory. *J. Chem. Phys.* **2008**, *129*, No. 034107.
(104) Mahler, A.; Janesko, B. G.; Moncho, S.; Brothers, E. N. When Hartree-Fock Exchange Admixture Lowers DFT-Predicted Barrier Heights: Natural Bond Orbital Analyses and Implications for Catalysis. *J. Chem. Phys.* **2018**, *148*, No. 244106.
(105) Lynch, B. J.; Truhlar, D. G. Robust and Affordable Multicoefficient Methods for Thermochemistry and Thermochemical Kinetics: The MCCM/3 Suite and SAC/3. *J. Phys. Chem. A* **2003**, *107*, 3898−3906.
(106) Lynch, B. J.; Truhlar, D. G. Small Representative Benchmarks for Thermochemical Calculations. *J. Phys. Chem. A* **2003**, *107*, 8996−8999.
(107) Lynch, B. J.; Truhlar, D. G. What Are the Best Affordable Multi-Coefficient Strategies for Calculating Transition State Geometries and Barrier Heights? *J. Phys. Chem. A* **2002**, *106*, 842−846.
(108) Fast, P. L.; Corchado, J.; Sanchez, M. L.; Truhlar, D. G. Optimized Parameters for Scaling Correlation Energy. *J. Phys. Chem. A* **1999**, *103*, 3139−3143.

https://doi.org/10.1021/acs.jpca.1c01695
J. Phys. Chem. A 2021, 125, 6474−6485